Trapped magnetic field distribution above a superconducting linear Halbach array

M Houbart[1], J-F Fagnard[1], J Dular[1], A R Dennis[2], D K Namburi[2,3], J H Durrell[2], C Geuzaine[1], B Vanderheyden[1] and P Vanderbemden[1]

[1] University of Liege, Department of Electrical Engineering and Computer Science, B-4000 Liege, Belgium
[2] University of Cambridge, Bulk Superconductivity Group, Cambridge CB2 1PZ, United Kingdom
[3] Quantum Sensors Group, James Watt School of Engineering, University of Glasgow, Glasgow G12 8QQ, United Kingdom

E-mail: michel.houbart@uliege.be

Abstract. In applications requiring a large magnetic force, permanent magnets with non-parallel magnetization directions can be assembled in a Halbach array to generate a large gradient of magnetic flux density. The saturation magnetization of permanent magnets, however, brings a fundamental limit on the performance of this configuration. In the present work, we investigate experimentally the assembly of cuboid bulk, large grain melt-textured $YBa_2Cu_3O_{7-x}$ superconductors ($\sim$14×14×14 mm^3) with orthogonal *c*-axes so as to form a basic unit of Halbach array. The experiments are carried out at 77 K.

The experimental distribution of the magnetic flux density above the array of trapped-field superconductors is compared to a similar array made of permanent magnets. A simple analytical model is developed and is shown to accurately reproduce the main experimental observations. The results suggest that a redistribution occurs in the current flowing in the central sample when the distance between the superconductors is reduced, whereas the neighbouring superconductors are unaffected. It is shown that this current redistribution yields a reduced contribution of the central sample to the magnetic flux density above the centre of the array and a new negative contribution associated with stray fields to the magnetic flux density at this location. This interpretation is confirmed by modelling of the distribution of transport currents in the superconductor using a 3D finite element model.

Bulk superconductor, trapped field magnet, magnetic field gradient, interacting bulk superconductors, flux pinning

1. Introduction

The force acting on a magnetic material results both from the magnitude and the gradient of the magnetic flux density $\vec{B}$. Applications involving such a force range from large lifting electromagnets down to magnetic matrices machined at the micrometre scale to attract fine magnetic particles [1], depending on the length scale of the gradient. In this work, we consider a compact system producing a magnetic gradient on the centimetre scale typical of magnetic drug delivery applications [2].
Two different methods are typically considered to generate the gradient. The first is the use of a "Halbach array" which consists of an assembly of permanent magnets with non-parallel magnetization which leads to an increase in the magnetic flux density on one side of the assembly. Recent work has aimed to optimize an array of neighbouring Nd-Fe-B to increase the gradient while taking into account the repelling forces during the assembly process [3–6]. Although other Halbach arrangements exist, the most common configuration corresponds to the case in which the magnetizations of neighbouring permanent magnets are perpendicular. This corresponds to the configuration investigated in this work. The second method involves taking advantage of the magnetic flux density gradient resulting from the insertion of a soft ferromagnetic material in a large uniform DC field. This "dipole field navigation" technique was successfully demonstrated in 2015 [7]. One advantage of this second method is that the large uniform DC field can also be used to fully magnetize the nanoparticles to be guided [8]. In both above mentioned methods however, the saturation magnetization $\mu_0 M_{sat}$ of the magnetic material used (1.4 T for Nd-Fe-B permanent magnets [9, 10] and 2.4 T for soft ferromagnetic Fe-Co alloys [11]) limits the maximum achievable field and field gradient.

In this context, the ability of bulk superconductors to trap large magnetic fields is of great interest as they can be employed as pseudo-permanent or "trapped-field" magnets. The trapped field of such magnets can be enhanced by increasing their dimensions [12, 13] and is not limited by any saturation magnetization. The maximum field trapped in a bulk superconductor to date is 17.6 T [14], almost one order of magnitude higher than the fundamental limit for iron. Instead of bulk materials, a stack of thin superconducting tapes can also be very efficient in trapping a field. It has been shown that these "quasi bulks" are also able to reach a trapped field in excess of 17 T [15].
With such values, magnetized superconductors are an attractive alternative for permanent magnets in applications requiring a large flux density $\vec{B}$ or a large gradient of flux density $\nabla||\vec{B}||$ [16–23]. In particular, magnetic drug delivery was demonstrated using two separated bulk superconductors with parallel magnetizations [24–26], or under a DC field, using a "zebra" architecture of alternated superconductors and ferromagnets to generate the required gradients [27].
In this work, we experimentally evaluate the combination of several cuboid superconductors in a Halbach configuration. The assembly process is more critical than for a classic Halbach array given that the trapped current loops in each magnetized sample may be altered by the proximity of another sample. The magnetization of two neighbouring superconductors in the array being perpendicular, the situation is actually comparable to a "crossed-field" configuration, in which the trapped field of a superconductor is affected by an external magnetic field which is not parallel to the main axis of magnetization [28–36].
In a few reports, the placement of several trapped field superconductors in close proximity was investigated [37]. A DC field varying sinusoidally in space was generated through the use of two staggered rows of stationary samples with parallel magnetizations [38–40]. A magnetic concentration effect was successfully demonstrated by exploiting flux trapping together with flux exclusion with samples having different critical temperatures [41, 42]. A circular Halbach array of superconductors for rotating machines was proposed and designed by Hull *et al* [43]. Experiments involving the combination of several superconducting magnets with perpendicular magnetizations however remains unexplored and is studied in details in this paper.

2. Experimental methods

In order to study the feasibility and the effectiveness of a superconducting Halbach array made of three magnetized cuboid superconductors we first consider the development and design of the experimental system. This system should allow the clamping of pre-magnetized superconducting magnets, their reproducible motion and the measurement of the properties of the resulting Halbach array. The most

relevant constraints considered during the design of the experimental system are listed below:

- The cryogenic temperature required is achieved by keeping the bottom part of the system in a liquid nitrogen bath. The experimental system uses Permaglas M730 for the parts partially immersed in liquid nitrogen, while the rest of the system including the motors, aluminum mechanical guides, and position sensors are maintained at room temperature above the cryogenic bath. This results in safer manipulations for the user and mitigates the problems related to thermal expansion of the precise translation and positioning mechanism.
- Due to large flux density trapped in the superconductors, significant magnetic forces are expected to develop within the array. The system, therefore, has to generate a translational motion of trapped field superconducting magnets over a range of 20 cm while handling safely the significant repulsive forces between the superconductors. These forces are evaluated numerically to exceed 60 N for an array of permanent magnets having individual remnant magnetization comparable to the typical trapped field at 77 K of the bulk $YBa_2Cu_3O_{7-x}$ cuboid superconductors used in this work. It should be highlighted that these repulsive forces develop mainly in a direction perpendicular to the axis of the array.
- Low magnetic susceptibility is required for the structure to avoid any magnetic interaction other than that occurring between the superconducting samples. For this reason, the sample holders are machined in aluminum ($\chi \sim 10^{-5}$).

A view of the experimental system fulfilling the above requirements is presented in Figure 1.

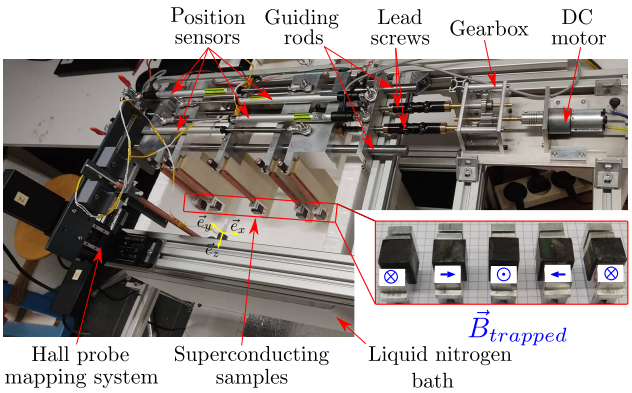

Figure 1. Picture of the experimental rig used to assemble and measure a linear Halbach array.

Figure 1 shows how the system is made up of five different carriages, allowing five magnets to be accommodated. The central carriage is fixed while the other four can be moved by activating two different trapezoidal lead screws. The motion of these four carriages is guided by two rods. Their positions are precisely measured with potentiometers. A gearbox allows the selection of the activated lead screw. A sample holder system intended to be immersed in liquid nitrogen is mounted on each carriage. Although the system was designed to allow the manipulation of five samples, only Halbach arrays made up of 3 samples were investigated in this work.

A Hall probe mapping system equipped with a cryogenic Hall sensor is incorporated into the experimental rig so that trapped field measurements can easily be performed on the assembled superconducting Halbach array. More specifically, during each experiment a mapping of the magnetic flux density is performed in a plane parallel to the surface of the configuration at a distance of 1 mm from the surface of the central sample. The distribution of the magnetic flux component perpendicular to the array (B_z) along the alignment direction (line x) is extracted from this mapping and shown for each case. The position of the mapping plane with respect to the studied configuration is presented schematically in Figure 2.

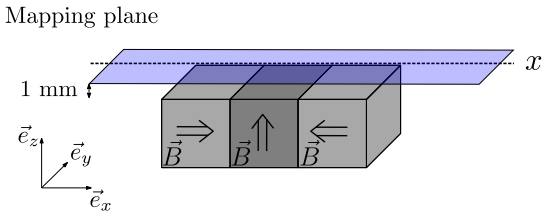

Figure 2. Schematic representation of the Hall probe mapping performed on the assembled array in each experiment. The samples represented here can either be permanent magnets or trapped field magnets.

The experimental system was first tested by assembling a classical Halbach array made up of three cubic ($12\times12\times12$ mm^3) Nd-Fe-B permanent magnets at ambient temperature. In this preliminary experiment, the permanent magnets were clamped in the experimental rig and the array was assembled by approaching the peripheral samples towards the central one at a speed of 0.6 mm s^{-1} until contact between them.

The superconducting $YBa_2Cu_3O_{7-x}$ samples investigated in this work were fabricated by the TSMG method [44–47]. The exact dimensions of the samples and their respective positions in the array are given in Table 1 and in Figure 3 respectively.

In the assembled array, each bulk superconducting sample was magnetized parallel to its c-axis, i.e the c-axis of sample 2 is parallel to the z-direction while the c-axes of samples 1 and 3 were respectively parallel

Table 1. Dimensions of the superconductors involved in the superconducting Halbach array.

Sample number	a_x [mm]	a_y [mm]	a_z [mm]
1	15.2	14.1	14.1
2	14.4	14.4	15.9
3	14.3	14.3	14.5

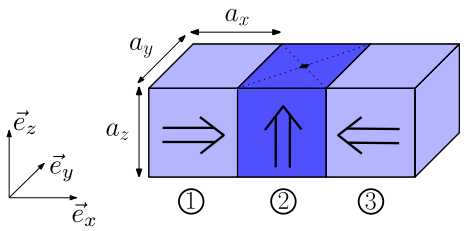

Figure 3. Position of the superconductors in the superconducting Halbach array.

and anti-parallel to the x-direction. Furthermore, the seed of sample 2 wad located on the side where the mapping is performed while the seeds of samples 1 and 3 were located on the faces in contact with sample 2.
The assembly of the superconducting Halbach array was achieved by first magnetizing each sample, one after the other at 77 K using a field cooling procedure from 1.2 T. The applied field was parallel to the c-axis of the superconductor and removed at a constant rate of 1 mT s^{-1}. At the end of the magnetization of the third sample, a period of 45 minutes was allowed for magnetic relaxation. The samples were then inserted and clamped in the experimental rig shown in Figure 1. At this point, the distance separating each sample ($\sim$ 80 mm) was large enough to assume no interactions between them [48]. The array was assembled by moving the external samples towards the central one at a speed of 0.6 mm s^{-1} until the three samples were in contact. A second period of 45 minutes was then allowed to let further magnetic relaxation occur before measuring the flux density distribution above the assembled array, as described above.

3. Models

3.1. Analytical Model

A simple analytical model allowing the computation of the 3 components of the magnetic flux density generated by cubic permanent magnets can be derived. This model assumes that the field generated by a cubic permanent magnet can be modelled by a surface current density, $\vec{K}$, flowing at the surface of the magnet.
Let us first consider the magnetic flux density generated by a quarter of a permanent magnet carrying a surface current of amplitude K_c. More particularly, let us consider two different current lines containing respectively the points $\vec{k}$ and $\vec{k} + \mathrm{d}z\vec{e}_z$ both located on the surface of the magnet. These lines define a surface carrying a total current $\vec{I} = K_c \mathrm{d}z \vec{e}_y$ as represented in Figure 4 (a).

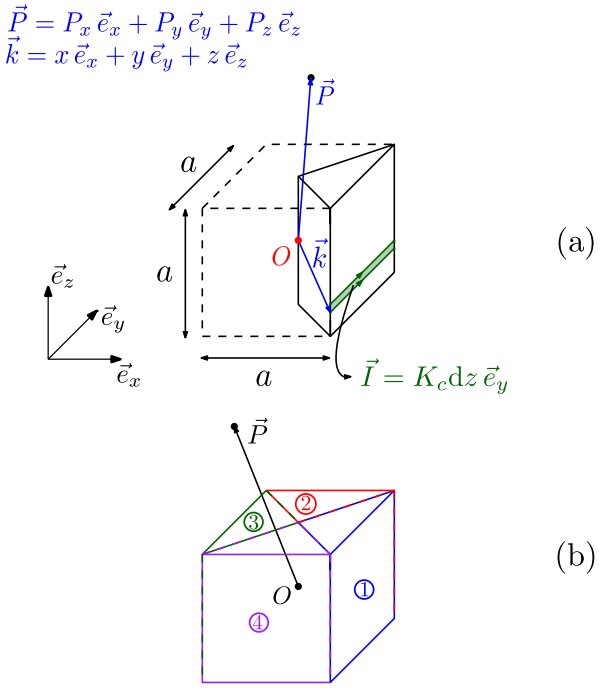

Figure 4. (a) Schematic representation of the analytical model of a quarter of a permanent magnet, (b) Numbering of the four quarters of permanent magnet.

It is assumed that the magnetic flux density $\mathrm{d}\vec{B}$ generated by the green surface in Figure 4(a) at point $\vec{P}$ can be computed with the Biot-Savart law, which writes:

$$\mathrm{d}\vec{B} = \frac{\mu_0 K_c}{4\pi} \int_{-\frac{a}{2}}^{\frac{a}{2}} \frac{\vec{e}_y \times (\vec{P} - \vec{k})}{||\vec{P} - \vec{k}||^3} \mathrm{d}y\,\mathrm{d}z. \quad (1)$$

The magnetic flux density generated at point $\vec{P}$ by the quarter of permanent magnet can thus be computed by integrating the expression (1) over the height of the cube.

$$\vec{B} = \frac{\mu_0 K_c}{4\pi} \int_{-\frac{a}{2}}^{\frac{a}{2}} \int_{-\frac{a}{2}}^{\frac{a}{2}} \frac{\vec{e}_y \times (\vec{P} - \vec{k})}{||\vec{P} - \vec{k}||^3} \mathrm{d}y\,\mathrm{d}z. \quad (2)$$

Noting $\alpha^2(x,z) = (P_x - x)^2 + (P_z - z)^2$ and solving (2) for the x and z-components one can obtain the relations (10) and (11) presented in appendix. The magnetic flux density generated by the full permanent magnet can then be computed simply by adding the contributions of each quarter. The number assigned to

each quarter and the expression of the total magnetic flux density is presented in Figure 4(b) and in equations (3) to (7) respectively.

$$\vec{B}_1 = f(P_x, P_y, P_z)\vec{e}_x + g(P_x, P_y, P_z)\vec{e}_z, \quad (3)$$
$$\vec{B}_2 = f(P_y, -P_x, P_z)\vec{e}_y + g(P_y, -P_x, P_z)\vec{e}_z, \quad (4)$$
$$\vec{B}_3 = -f(-P_x, -P_y, P_z)\vec{e}_x + g(-P_x, -P_y, P_z)\vec{e}_z, \quad (5)$$
$$\vec{B}_4 = -f(-P_y, P_x, P_z)\vec{e}_y + g(-P_y, P_x, P_z)\vec{e}_z, \quad (6)$$
$$\vec{B}_{tot} = \vec{B}_1 + \vec{B}_2 + \vec{B}_3 + \vec{B}_4. \quad (7)$$

A similar procedure was applied to compute analytically the magnetic flux density generated by a magnetized cubic bulk superconductor. The model considers a completely magnetized superconductor in the critical state (Bean model [49]) with square current loops strictly parallel to the $a-b$ planes. The model also assumes that the critical current density is a constant, field-independent value equal to J_c over the whole superconductor. Let us consider the magnetic flux density generated by a quarter of this superconductor, as shown schematically in Figure 5 (a). More particularly, let us consider four different current lines containing respectively the points $\vec{k}$, $\vec{k} + \mathrm{d}x\vec{e}_x$,$\vec{k} + \mathrm{d}y\vec{e}_y$ and $\vec{k} + \mathrm{d}x\vec{e}_x + \mathrm{d}z\vec{e}_z$. These lines define a volume carrying a total current $\vec{I} = J_c\,\mathrm{d}x\mathrm{d}z\vec{e}_y$ as represented in Figure 5 (a).

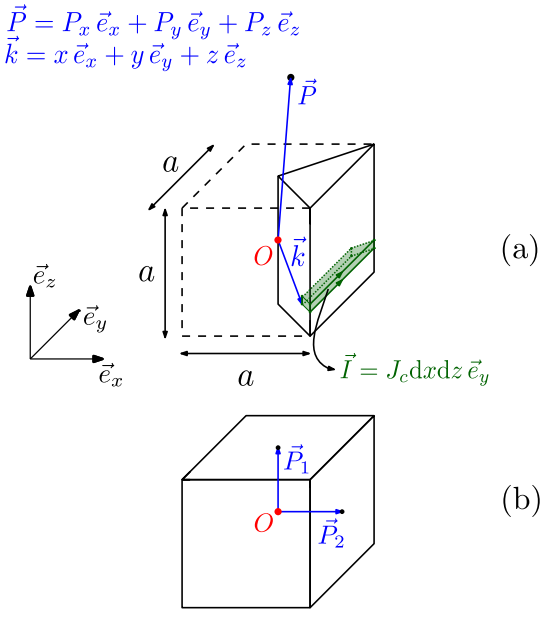

Figure 5. (a) Schematic representation of the analytical model of a quarter of a superconductor, (b) Position of the points $\vec{P}_1$ and $\vec{P}_2$.

It is assumed that the magnetic flux density $\mathrm{d}\vec{B}$ generated by the volume shown in green in Figure 5(a) at the point $\vec{P}$ can be computed with the Biot-Savart law. Similarly to the calculation done for permanent magnets, this expression can be integrated over the quarter of superconductor to compute the flux density at point $\vec{P}$, which writes:

$$\vec{B} = \frac{\mu_0}{4\pi}\int_0^{\frac{a}{2}}\int_{-\frac{a}{2}}^{\frac{a}{2}}\int_{-\frac{L(x)}{2}}^{\frac{L(x)}{2}} J_c\,\frac{\vec{e}_y \times (\vec{P}-\vec{k})}{||\vec{P}-\vec{k}||^3}\,\mathrm{d}y\,\mathrm{d}z\,\mathrm{d}x, \quad (8)$$

where $L(x)$ is the length of the current line containing the point $\vec{k}$. In the case of a cubic superconductor in the critical state, $L(x) = 2x$.

The first two integrals appearing in equation (8) are similar to those for permanent magnets. The x and z-components of the magnetic flux density thus take the integral form presented in equations (12) and (13) in appendix. The total magnetic flux density can be computed by applying the equations (3) to (7) with the functions f^* and g^* instead of f and g. This expression can be simplified at two particular points exploiting the different symmetries of the generated flux density. The first point $\vec{P}_1$ corresponds to the geometrical centre of the top surface of the cube; the second point $\vec{P}_2$ corresponds to the geometrical centre of a lateral surface. At these points, only the z-component of the flux density does not vanish and their values can be computed semi-analytically using the equations (14) and (15) (given in appendix). From these equations, the ratio $B_z^{P_2}/B_z^{P_1}$ is found not to depend on the critical current density of the sample nor on its size. It only depends on the aspect ratio of the superconductor, for a cube, $B_z^{P_2}/B_z^{P_1}$ is equal to $0.16 \simeq 1/6$.

It should be highlighted that the model presented in this section can easily be extended to parallelepiped samples by inserting integration bounds in equations that are not equal to each other, i.e. $a_x \neq a_y \neq a_z$, in equations (2) or (8). Also, it is possible to take into account a possible variation of J_c along the c-axis of the superconductor by incorporating this dependence in equation (8).

3.2. Finite element model

In order to obtain a deeper understanding of the physical phenomena arising during the assembly process, a numerical tool was developed in the *GetDP* environment. Starting from the "A-formulation" developed in [50], the code was extended to investigate the interaction between several magnetized bulk superconductors in relative motion with respect to each other. The modelling of the motion is performed by updating the position of the superconducting regions at each time step and by projecting the A-field computed at the previous time step in these regions. The remeshing of the domain required by such an approach increases

significantly the numerical cost of the method, which prevents us from using a fine mesh to solve the problem. Given the absence of symmetry, a 3D modelling should be carried out. In order to keep a reasonable computation time, the size of the mesh inside the superconducting regions is around 1/12 of the cube side a ($\sim$ 1 mm). The purpose of the simulations consists in the qualitative understanding of the phenomenon occurring during the assembly rather than obtaining a quantitative agreement with experimental results.
The zero field cooling magnetization of an individual cubic superconductor (14×14×14 mm^3) is first simulated to compute the initial A-field distribution. The temperature of the superconductor is assumed to be constant (77 K) for the modelling. The magnetization process, therefore, is assumed to be carried out in zero-field cooled mode, with a maximum field equal to 2.4 T, i.e. twice the magnetizing field used in the experimental field cooled procedure. During this magnetization process, the field is increased and then decreased at a constant rate of 1 mT s^{-1}. The critical exponent is fixed to a typical value for $YBa_2Cu_3O_{7-x}$ bulk superconductors at 77 K: $n = 20$ [51]. The average critical current density is fixed to 2.3×10^8 A m^{-2} so that after 45 minutes of magnetic relaxation, the remaining current density flowing in the superconductor is close to the value deduced experimentally. The critical current density is also assumed to be homogeneous and isotropic. Two cases are considered : (i) a field-independent J_c or (ii) a field-dependent $J_c(\vec{B})$ following a Kim dependence [52] considered as:

$$J_c(\vec{B}) = J_{c0}\,\frac{1}{1+||\vec{B}||/B_0}. \qquad (9)$$

In this case, the parameter B_0 is chosen equal to 0.5 T, in agreement with $J_c(\vec{B})$ behavior reported at 77 K for other bulk melt-textured $YBa_2Cu_3O_{7-x}$ samples [53]. The value of J_{c0} is adjusted so as the field-averaged J_c between 0 and 1.2 T, i.e. the maximum flux density experienced by the superconducting sample during the experiment is equal to the field-independent value, i.e. 2.3×10^8 A m^{-2}.
The initial A-field distribution before any relative motion of the superconductor is evaluated 45 minutes after the end of the magnetization. The assembly process of three identical cubic magnetized bulk superconductors in a Halbach array is then simulated as follows. The initial distance separating each bulk from its neighbour is set to 40 mm and the individually computed A-field distributions are projected in each sample. The separating distance is then reduced at a rate of -1 mm s^{-1} until it reaches a value of 0.5 mm.

4. Results and discussion

We now move to the experimental results which are divided in three parts. First, an individual characterization of the samples used throughout the work is presented. Secondly, measurements performed on a Halbach array made up of three cubic (12×12×12 mm^3) Nd-Fe-B permanent magnets at ambient temperature are presented. The investigation of this well-known configuration will allow us to highlight the characteristics that are specific to superconducting trapped field magnets later on. Finally, we focus on the experiments performed at 77 K to assess the feasibility of assembling a Halbach array made of 3 magnetized cuboid $YBa_2Cu_3O_{7-x}$ bulk superconductors.

4.1. Characterization of individual magnets

A Hall probe mapping is performed for each Nd-Fe-B permanent magnet at ambient temperature 1 mm away from the surface of the sample. The value of K_c used in equation (11) is adjusted to obtain the best agreement between experimental data and analytical predictions. This leads to $K_c = 10^6$ A m^{-1} for all the samples. Considering this surface current, the permanent magnets are expected to exhibit a magnetic moment m equal to 1.77 A m^2. This value is confirmed experimentally through the direct measurement of the magnetic moment using a bespoke flux extraction magnetometer able to accommodate magnetized samples of large size [54].

Preliminary trapped field measurements are then performed on each cuboid superconductor considered in this work. After the magnetization process described in Section 2, a period of 45 minutes is allowed for magnetic relaxation and the trapped field is measured on both sides of the sample. The trapped flux density value at the centre of the top and bottom faces of each sample are shown in Table 2.

Table 2. Trapped field value at 77 K for the three investigated bulk superconductors. The top surface corresponds to the surface including the seed.

Sample number	Trapped field 1 mm over the top surface [mT]	Trapped field 1 mm over the bottom surface [mT]
1	440	112
2	466	145
3	461	98

A striking feature that can be observed for each sample in Table 2 is the noticeable difference between the trapped field measured above the two opposite surfaces of the superconductor. This observation can

be explained by a progressively decreasing J_c away from the seed of the sample, as an inhomogeneous J_c is sometimes found for melt-textured (RE)BCO superconductors [55–57]. In this work, we use a simplified approach which consists in considering a critical current varying along the c-axis in order to approximate the trapped flux density both on top and bottom faces of the sample. Further details concerning the considered evolution of the critical current density along the c-axis are given in appendix. Using the adjusted analytical model, the maximum flux density trapped inside the superconductors is found to be equal to 1.2 T. This results highlights that a field cooling process under 1.2 T is enough to fully magnetize the bulk superconductors to be used in the Halbach array. Note that due to the non homogeneous J_c distribution along the c-axis, the maximum magnetic flux density is not reached at the geometrical centre of the sample within this model.

4.2. Halbach array with 3 permanent magnets

Three permanent magnets are assembled at ambient temperature in a Halbach array using the experimental procedure described in Section 2. Figure 6 shows the measured magnetic flux density distribution along the line x at 1 mm above the top surface of the Halbach array. The measurements are also compared to the predictions of the analytical model described in Section 3.1. In this configuration, the model assumes a simple vector summation of the flux density generated by each permanent magnet in the array and that no alteration of the individual magnetization is considered.
As can be seen from the data represented in Figure 6, the analytical model predicts very appropriately the magnetic flux density distribution measured experimentally. This observation gives evidence that the Halbach configuration including 3 Nd-Fe-B permanent magnets can be seen as the simple addition of the individual and independent contributions of the flux density generated by each magnet. This result is expected since the applied field $\mu_0 H$ should typically exceed 1 T to observe irreversible demagnetization of Nd-Fe-B magnets [58], which is much larger than the stray fields ($\sim$ 500 mT) of the permanent magnets used. As expected for Halbach arrays, this summation of individual contributions leads to an increase of 30% of both the maximum value of the magnetic flux density reached and the magnetic flux density gradient generated 1 mm away from the array.

4.3. Halbach array with 3 bulk superconducting magnets

In this section we investigate the three cuboid bulk superconductors characterized previously now

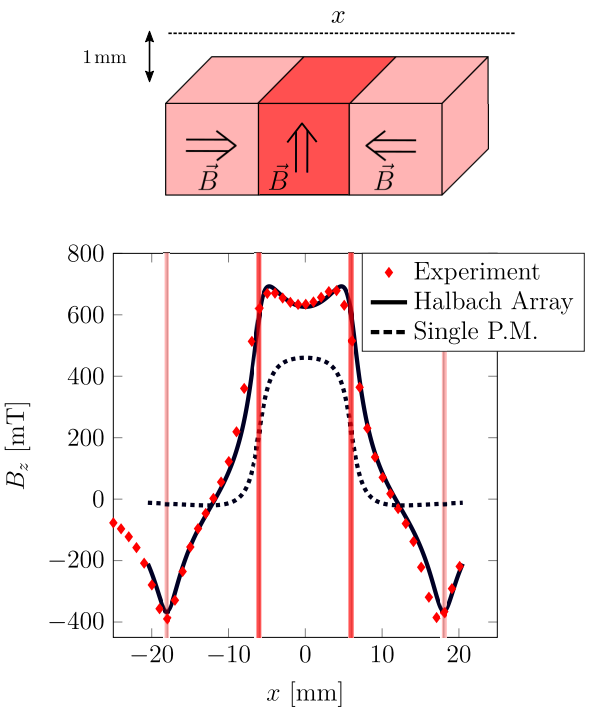

Figure 6. Evolution of the z-component of the magnetic flux density generated 1 mm away from the surface of a single Nd-Fe-B permanent magnet and of a Halbach array made up of three Nd-Fe-B permanent magnets along the line x. The red vertical lines are located at the border of the samples. The experimental data are compared to an analytical model assuming a simple vector summation of the flux densities generated by each permanent magnet in the array and no alteration of the individual magnetization.

combined in a linear Halbach array. Both numerical and experimental approaches are investigated and the main difference with Nd-Fe-B permanent magnets are highlighted.

4.3.1. Modelling We first examine the current density inside the bulk superconductor determined using the 3D finite element model described in Section 3.2. Figure 7 compares the current density distributions before and after the assembly process of the array when the critical current density J_c is assumed to be field-independent. This comparison is carried out in two different planes. Plane 1 (shown in red in Figure 7) includes the c-axis of the central sample and the centres of all the samples. Plane 2 (shown in green in Figure 7) is parallel to the contact surface between the samples and cuts the central sample at 0.1 mm from its edge.

As can be observed in Figure 7, the finite element simulation predicts a reorganisation of the current density distribution inside the samples during the assembly process. More particularly, this reorganisation is expected to occur only in a region close to the contact surface between neighbouring samples. In the

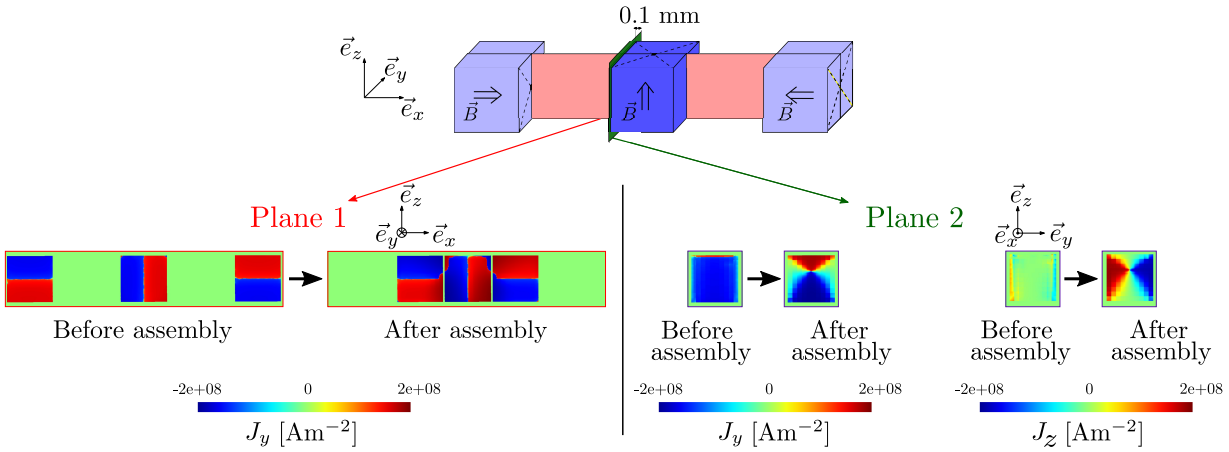

Figure 7. Comparison of the y and z-components of the current density distribution before and after the assembly of the superconducting Halbach array computed by the finite element model. A field-independent critical current density of 2.3×10^8 A m^{-2} is considered in this simulation.

simulation this region is found to be only one finite-element thick, the actual thickness is thus expected to be smaller or equal to 1 mm. The numerical confirmation of this value would require a refinement of the mesh in the superconducting regions, which would dramatically increase the numerical cost of the simulation. An alternative way of determining this thickness with the analytical model will thus be proposed in the next section.

A qualitative understanding of the current distribution after the assembly process may already be extracted from the results in Figure 7. We first look at the results in the central sample. Before the assembly, the current distribution in this sample is close to the distribution expected for the critical state, i.e. a uniform current density for which Plane 1 is shared symmetrically with positive and negative values. The situation changes significantly when the samples are in close vicinity, especially in regions close to the neighbouring superconducting samples. As appears from the results in Plane 2, the supercurrents close to the sample borders flow in loops that are perpendicular to the x-axis after the assembly of the array, i.e. perpendicular to the direction of magnetization in the two neighbouring samples. The z-component of the magnetic flux density generated by these regions over the centre of the array is thus smaller than before assembling the configuration. In addition, these modified current loops are found to oppose the field generated by the closest neighbouring sample. This redistribution is expected to have two consequences: (i) a decrease in the contribution of the central sample to the magnetic flux density above the centre of the array, and (ii) the apparition of a new negative contribution to the magnetic flux density at this location.

From the results shown in Figure 7, it can also be noticed that the current distribution in the peripheral samples is much less affected than the current in the central sample during the assembly process. The current loops in these samples are found to remain mostly perpendicular to the x-axis and are close to their initial distribution. This much smaller impact on the current distribution of the two peripheral samples may be understood considering that beside its own trapped field, the only significant field contribution experienced by a peripheral sample during the assembly process corresponds to the return field lines associated to the trapped field of the central sample. From the results obtained in Section 3.1, this contribution is expected to be approximately 6 times smaller than the trapped field of the central sample, regardless of the particular value of the critical current density. The situation is completely different for the central sample which is aligned with the c-axis of the peripheral samples and is thus subjected, at the end of the assembly process, to a maximum field amplitude equal to the trapped field at the centre of their top surfaces.

A second finite element simulation introducing this time the critical current density dependency upon the magnetic flux density in the model is then performed. The current density distributions computed before and after the assembly process in Plane 1 and 2 are presented in Figure 8. From the results presented in Figure 8, it can be observed that taking into account a relatively strong field dependence of J_c as the one reported in equation (9), instead of a constant J_c, does not bring any qualitative change to the conclusions of this finite element study.

4.3.2. Experimental results The experimental assembly process and the measurement method followed in this experiment are presented in Section 2. The first model to which measurements of the flux distribution above the array are compared assumes that the mag-

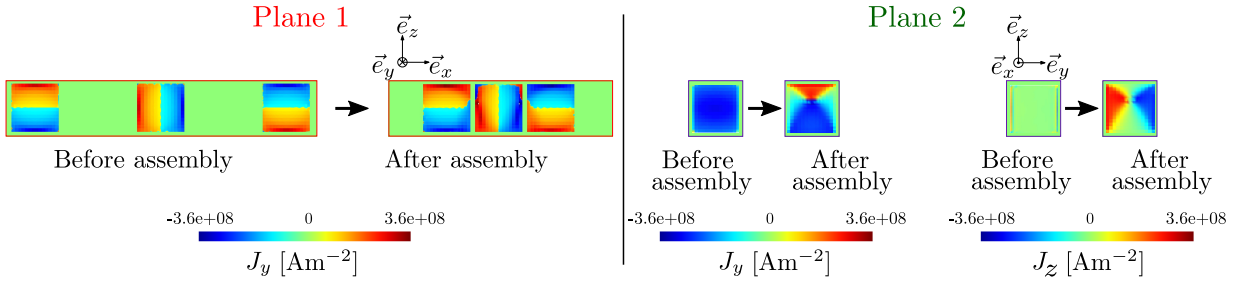

Figure 8. Comparison of the y and z-components of the current density distribution before and after the assembly of the superconducting Halbach array computed by the finite element model. The considered field dependence of the critical current density is given in equation (9), with $J_{c0} = 4.5 \times 10^8$ A m^{-2} and $B_0 = 0.5$ T.

netized bulk superconductors behave similarly to permanent magnets during the assembly of the array. The current density distribution in each superconductor is thus assumed to remain unchanged even after having brought the superconductors in close vicinity. Figure 9 presents a comparison between the magnetic flux density distribution, measured at 77 K, 1 mm away from the surface of the array and the sum of the individual contribution of each sample computed with the analytical model described in Section 3.1. Note that the model takes into account the inhomogeneous distribution of J_c in each sample.

As observed in Figure 9, the agreement with experimental data is good above the peripheral samples of the array. However, it may be noted that the model assuming no alteration of the individual magnetization significantly overestimates the maximum flux density generated above the centre of the superconducting Halbach array; the maximum field measured experimentally is 471 mT, i.e. only 5 mT higher than the trapped field of sample 2, while the analytical model assuming no modification of current density in the central sample predicts a field of 530 mT. The contribution of samples 1 and 3 to the magnetic flux density over the centre of the array thus appears to be rather small, unlike the Halbach array made of Nd-Fe-B permanent magnets. This observation can be compared with the predictions of the finite element model, suggesting that the current density distribution of the central superconductor is modified during the assembly process.

In order to improve the agreement with the experimental magnetic flux distribution, the analytical model used to compute the magnetic flux density generated by the array is then modified with a slightly different current density distribution. Based on the qualitative observations performed with the finite element model, it is assumed that the interactions between the samples result in a current redistribution occuring in two zones of equal thickness e on both sides of the superconductor located at the centre of the array, as shown schematically in Figure 10. In these zones, the current is modelled to flow in loops perpendicular to the x direction in such a way that it opposes the contribution of the closest neighbouring sample. The current density there is also assumed to be field-independent and anisotropic, i.e. the current density in the z-direction is three times smaller than the value $J_{c,max}$ of the central superconductor (sample 2). This anisotropy leads to a more elaborated current distribution in these zones as represented schematically in Figure 10 [59, 60]. The magnetic flux density generated along the line x by such a distribution is then computed for several values of the thickness e. The results are compared to the

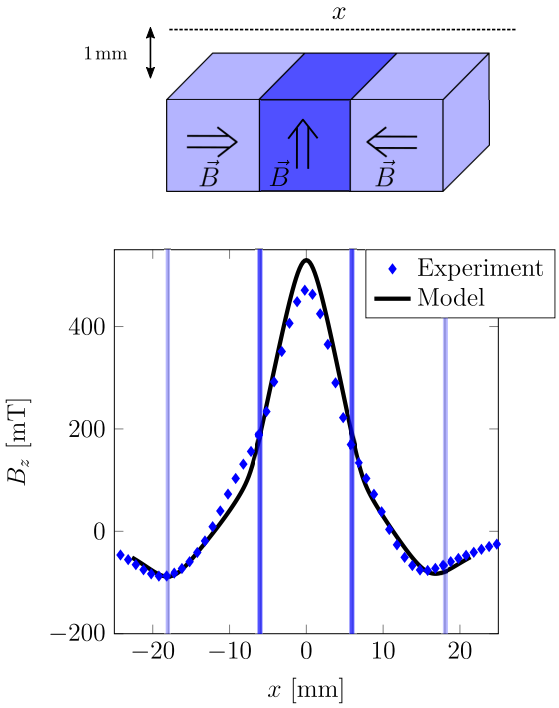

Figure 9. Evolution of the z-component of the magnetic flux density generated 1 mm away from the surface of a Halbach array made up of three cuboid bulk superconductors along the line x. The blue vertical lines are located at the border of the superconducting samples. The experimental data are compared to an analytical model assuming a simple vector summation of the flux densities generated by each superconductors in the array and no alteration of the individual magnetization.

experimental data in Figure 11.

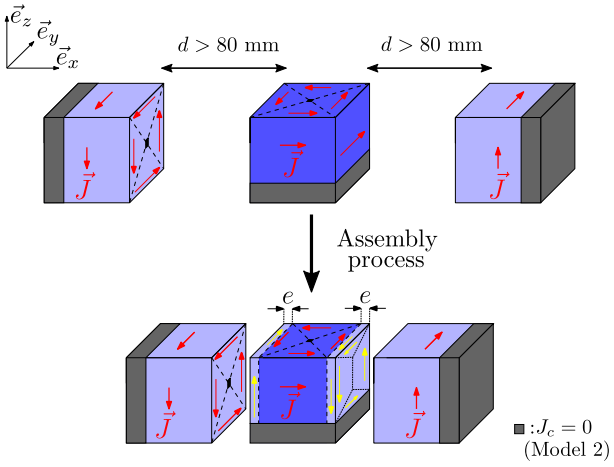

Figure 10. Schematical representation of the analytical model of a superconducting Halbach array accounting for the samples interactions. The red arrows shows the current distribution in the samples before assembling the array while the yellow arrows shows the modifications induced by the interaction during the assembly process.

It is observed in Figure 11 that for values of e ranging from 0 to 2 mm, the magnetic flux density distribution over the peripheral superconductors is only weakly affected by the modification of the current distribution. Then focusing on the value of the field generated above the centre of the array, it can be noticed that increasing the thickness e of the zones where the current distribution is altered leads to a decrease of this central field. The value of the thickness e can thus be adjusted in order to fit the central field value measured experimentally while conserving a good agreement above the peripheral sample. From Figure 11, it appears that a thickness $e = 0.8$ mm leads to a fair agreement between experimental results and analytical predictions. It should be emphasized that the computed value of e is smaller than 1 mm as expected by the finite element simulation.

In practice, the current density distribution is likely to be more elaborated than the simplified picture shown in Figure 10. Nevertheless, this very simple approach allows the determination of the thickness e effortlessly and is able to capture effectively the main features of the actual magnetic flux density generated by a superconducting Halbach array. The analytical computations also seem to confirm that the main obstacle to the applicability of superconducting Halbach array is linked to a demagnetization of the central superconductor during the assembly of the configuration.

Finally, it should be noticed that the flux distribution over the central superconductor is weakly affected by the non-uniform distribution of J_c. This is shown in Appendix 2, where the above results are compared to those obtained using a constant value of the critical current density over the whole superconductor.

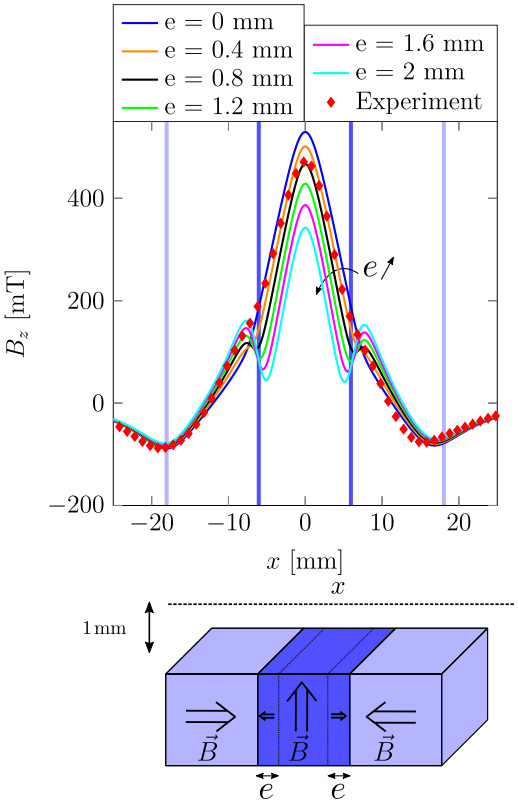

Figure 11. Evolution of the z-component of the magnetic flux density generated 1 mm away from the surface of a Halbach array made up of three cuboid bulk superconductors along the line x. The blue vertical lines are located at the border of the superconducting samples. The curves represent the predictions of the analytical model assuming a simple vector summation of the flux densities generated by each superconductor in the array. The model also assumes that during the assembly of the configuration the current distribution in the central sample is altered over two zones of equal thickness e as represented schematically in Figure 10.

5. Conclusions

The flux density distribution generated by a superconducting Halbach array comprised of $YBa_2Cu_3O_{7-x}$ bulk superconductors was investigated. An experimental system accommodating up to 5 cuboid samples and capable of overcoming the significant repulsive forces arising during the assembly of the array was designed. The system was used to successfully assemble and measure a superconducting Halbach array of 3 superconductors. Both finite element simulations and analytical calculations were compared to the measurements of the magnetic flux density distribution above the array of trapped field magnets.

It was found that the peripheral samples can be assumed to remain in the critical state despite the close vicinity of the central superconductor. However, the approach of the peripheral samples to the central sample during array assembly disturbs the current density distribution in the central superconductor. This alteration of the current distribution results in a reduction of the maximum magnetic flux density generated, limiting the performances of the array. Preventing the occurrence of this reorganization of current density would indeed lead to a situation where the maximum magnetic flux density generated at a distance of 1 mm is 13 % higher than that generated with a single superconductor. Given that the maximum field trapped in a superconductor to date is almost one order of magnitude higher than the saturation magnetization of permanent magnets, the same would be true when comparing the performance of superconducting with that of classic Halbach arrays. The remaining challenge, however, would consist in handling the repulsive force between the superconductors which scale with the square of the trapped field of individual magnets. Since the repulsive forces develop in a direction perpendicular to the axis of the array, it is to be noted that the main task is not really to reduce the distance between the magnetized superconducting samples, but to do so in such a way they are kept aligned with each other.
A simple analytical model assuming a field-independent critical current density and including the current density distribution modification was also adjusted, capturing successfully the main features of the $\vec{B}$-field measured experimentally. Finally, it was also shown that the unavoidable non-uniformity of J_c is not a major issue in this application.

Acknowledgment

This work was supported by the Fonds de la Recherche Scientifique - FNRS under grant CDR n° J.0218.20 (35325237). Michel Houbart is recipient of a FRS-FNRS Research Fellow grant.

References

[1] W Ge, A Encinas, E Araujo, and S Song 2017 *Results in Physics* **7** 4278–4286
[2] S Senapati, AK Mahanta, S Kumar, and P Maiti 2018 *Signal Transduct. Target. Ther.* **3** 7
[3] L C Barnsley, D Carugo, J Owen, and E Stride 2015 *Phys. Med. Biol.* **60** 8303–8327
[4] L C Barnsley, D Carugo, and E Stride 2016 *J. Phys. D: Appl. Phys.* **49** 225501
[5] H Kee, H Lee, and S Park 2020 *J. Magn. Magn. Mater.* **514** 167180
[6] A Omelyanchik, G Lamura, D Peddis, and F Canepa 2021 *J. Magn. Magn. Mater.* **522** 167491
[7] M Latulippe, and S Martel 2015 *IEEE Trans. Robot.* **31** 1353–1363
[8] M Latulippe, O Felfoul, P E Dupont, and S Martel 2016 *Appl. Phys. Lett.* **108** 062403
[9] F Fohr, and N Volbers 2018 *AIP Advances* **8** 047701
[10] D Brown, B-M Ma, and Z Chen 2002 *J. Magn. Magn. Mater.* **248** 432–440
[11] F Fohr, and N Volbers 2018 *AIP Advances* **8** 047701
[12] S Nariki, H Teshima, and M Morita 2016 *Supercond. Sci. Technol.* **29** 034002
[13] M Tomita, M Murakami 2003 *Letters to Nature* **421** 517–520
[14] J H Durrell, A R Dennis, J Jaroszynski, M D Ainslie, K G B Palmer, Y-H Shi, A M Campbell, J Hull, M Strasik, E E Hellstrom, and D A Cardwell 2014 *Supercond. Sci. Technol.* **27** 082001
[15] A Patel, A Baskys, T Mitchell-Williams, A McCaul, W Coniglio, J Hänisch, M Lao, and B A Glowacki 2018 *Supercond. Sci. Technol.* **31** 09LT01
[16] J H Durrell, M D Ainslie D Zhou, P Vanderbemden, T Bradshaw, S Speller, M Filipenko, and D A Cardwell 2018 *Supercond. Sci. Technol.* **31** 103501
[17] N Saho, N Nishijima, H Tanaka, and A Sasaki 2009 *Physica C Supercond.* **469** 1286–1289
[18] T Nakamura, D Tamada, Y Yanagi, Y Itoh, T Nemeto, H Utumi, and K Kose 2015 *J. Magn. Reson.* **259** 68–75
[19] M D Ainslie, A George, R Shaw, L Dawson, A Winfield, M Steketee, and S Stockley 2014 *J. Phys. Conf. Ser.* **507** 032002
[20] D Zhou, M Izumi, M Miki, B Felder, T Ida, and M Kitano 2012 *Supercond. Sci. Technol.* **25** 103001
[21] F N Werfel, U Floegel-Delor, R Rothfeld, T Riedel, B Goebel, D Wippich, and P Schirrmeister 2012 *Supercond. Sci. Technol.* **25** 014007
[22] K S Haran, S Kalsi, T Arndt, H Karmaker, R Badcock, B Buckley, T Haugan, M Izumi, D Loder, J W Bray, P Masson, and E W Stautner 2017 *Supercond. Sci. Technol.* **30** 123002
[23] F Mishima, S-I Takeda, Y Izumi, and S Nishijima 2006 *IEEE Trans. Appl. Supercond.* **16** 367–371
[24] S-I Takeda, F Mishima, S Fujimoto, Y Izumi, and S Nishijima 2007 *J. Magn. Magn. Mater.* **311** 367–371
[25] F Mishima, S-I Takeda, Y Izumi, and S Nishijima 2007 *IEEE Trans. Appl. Supercond.* **17** 2303–2306
[26] S Nishijima, S-I Takeda, F Mishima, Y Tabata, M Yamamoto, J-I Joh, H Iseki, Y Muragaki, A Sasaki, and K Jun, N Saho 2008 *IEEE Trans. Appl. Supercond.* **18** 874–877
[27] S B Kim, I Eritate, T Abe, M Takashashi, S Shima, and A Nakashima 2015 *IEEE Trans. Appl. Supercond.* **25** 4602704
[28] K Funaki, and K Yamafuji 1982 *Jpn. J. Appl. Phys.* **21** 299–304
[29] A M Campbell, M Baghdadi, A Patel, D Zhou, K Y Huang, Y-H Shi, and T A Coombs 2017 *Supercond. Sci. Technol.* **30** 034005
[30] Z Hong, P Vanderbemden, R Pei, Y Jiang, A M Campbell, and T A Coombs 2008 *IEEE Trans. Appl. Supercond.* **18** 1561–1564
[31] P Vanderbemden, Z Hong, T A Coombs, S Denis, M Ausloos, J Schwartz, I B Rutel, N Hari Babu, D A Cardwell, and A M Campbell 2007 *Phys. Rev. B* **75** 174515
[32] L M Fisher, A V Kalinov, S E Savel'ev, I F Voloshin, V A Yampol'skii, M A R Leblanc, and S Hirscher 1997 *Physica C Supercond.* **278** 169–179
[33] J Srpcic, F Perez, K Y Huang, Y-H Shi, M D Ainslie, A R Dennis, M Filipenko, M Boll, D A Cardwell, and J H Durell 2019 *Supercond. Sci. Technol.* **32** 035010
[34] J Luzuriaga, A Badía-Majós, G Nieva, C López, A Serquis, and G Serrano 2009 *Supercond. Sci. Technol.* **22** 015021
[35] M Kapolka, J Srpcic, D Zhou, M D Ainslie, E Pardo,

and A R Dennis 2018 *IEEE Trans. Appl. Supercond.* **28** 6801405
[36] J Srpcic, F Perez, K Y Huang, Y-H Shi, M D Ainslie, A R Dennis, M Filipenko, M Boll, D A Cardwell, and J H Durell 2019 *Supercond. Sci. Technol.* **32** 035010
[37] T Oka, Y Takahashi, S Yaginuma, J Ogawa, S Fukui, T Sato, K Yokoyama, and T Nakamura 2016 *Phys. Procedia* **81** 45–48
[38] R Kinjo, K Mishima, Y W Choi, M Omer, K Yoshida, H Negm, K Torgasin, M Shibata, K Shimahashi, H imon, K Okumura, M Inukai, H Zen, T Kii, K Masuda, K Nagasaki, and H Ohgaki 2014 *Phys. Rev. Accel. Beams* **17** 022401
[39] T Kii, R Kinjo, N Kimura, M Shibata, M A Bakr, Y W Choi, M Omer, K Yoshida, K Ishida, T Komai, K Shimahashi, T Sonobe, H Zen, K Masuda, and H Ohgaki 2012 *IEEE Trans. Appl. Supercond.* **22** 4100904
[40] S D Chen, C S Hwang, C M Yang, and I G Chen 2014 *IEEE Trans. Appl. Supercond.* **24** 4603005
[41] S Choi, J-H Yoon, B-S Lee, M-S Won, J-W Ok, Z Y Zhang, T Kiyoshi, S Matsumoto, S-H Lee 2012 *J. Appl. Phys.* **111** 07E728
[42] K Takahashi, H Fujishiro, M D Ainslie 2018 *Supercond. Sci. Technol.* **31** 044005
[43] J R Hull 1999 *IEEE Trans. Appl. Supercond.* **9** ASC98
[44] D A Cardwell 1998 *Mater. Sci. Eng. B Solid State Mater. Adv. Technol.* **53** 1–10
[45] Y-H Shi, D K Namburi, W Zhao, J H Durrell, A R Dennis, and D A Cardwell 2016 *Supercond. Sci. Technol.* **29** 015010
[46] D K Namburi, Y-H Shi, W Zhai, A R Dennis, J H Durrell, and D A Cardwell 2015 *Cryst. Growth Des.* **15** 1472–1480
[47] D K Namburi, Y Shi, and D A Cardwell 2021 *Supercond. Sci. Technol.* **34** 053002
[48] M Houbart, J-F Fagnard, A R Dennis, D K Namburi, Y Shi, J H Durrell, and P Vanderbemden 2020 *Supercond. Sci. Technol.* **33** 064003
[49] C P Bean 1962 *Phys. Rev. Lett.* **8** 250–253
[50] J Dular, C Geuzaine, and B Vanderheyden 2020 *IEEE Trans. Appl. Supercond.* **30** 8200113
[51] H Yamasaki, and Y Mawatari 2000 *Supercond. Sci. Technol.* **13** 202–208
[52] Y B Kim, C F Hempstead, and A R Strnad 1962 *Phys. Rev. Lett.* **9** 306–309
[53] K Berger, J Lévêque, D Netter, B Douine, and A Rezzoug 2007 *IEEE Trans. Appl. Supercond.* **17** 3028–3031
[54] R Egan, M Philippe, L Wera, J-F Fagnard, B Vanderheyden, A Dennis, Y Shi, D Cardwell, and P Vanderbemden 2015 *Rev. Sci. Instrum.* **86** 025107
[55] C D Dewhurst, W Lo, Y H Shi, and D A Cardwell 1998 *Mat. Sci Eng. B* **53** 169–173
[56] T Nakashima, J Shimoyama, M Honzumi, Y Tazaki, S Horii, and K Kishio 2005 *Physica C* **426-431** 720–725
[57] P Yang, J F Fagnard, P Vanderbemden, and W Yang 2019 *Supercond. Sci. Technol.* **32** 115015
[58] M Katter 2005 *IEEE Trans. Magn.* **41** 3853 – 3855
[59] P Vanderbemden, A D Bradley, R A Doyle, W Lo, D M Astill, D A Cardwell, and A M Campbell 1998 *Physica C Supercond.* **302** 257–270
[60] E M Gyorgy, R B Van Dover, K A Jackson, L F Schneemeyer, and J V Waszczak 1989 *Appl. Phys. Lett.* **55** 283–285

Appendix 1: Evolution of the critical current density along the *c*-axis

In this work, two different evolutions of the critical current density along the *c*-axis are investigated and incorporated in equation (8). The first corresponds to a linear variation of J_c between a value at the top surface ($J_{c,top}$) and another value at the bottom surface ($J_{c,bottom}$). The second corresponds to a constant critical current density ($J_{c,max}$) in the upper part of the superconductor followed by an abrupt drop to 0 at a given position along the *c*-axis. These two simplified (linear and step-like) $J_c(z)$ were considered for their simplicity. The parameters of both models are adjusted for each sample to obtain the best agreement with experimental data. As an illustration, the measured trapped field of sample 2 along the line x is compared to both models in Figure 12.

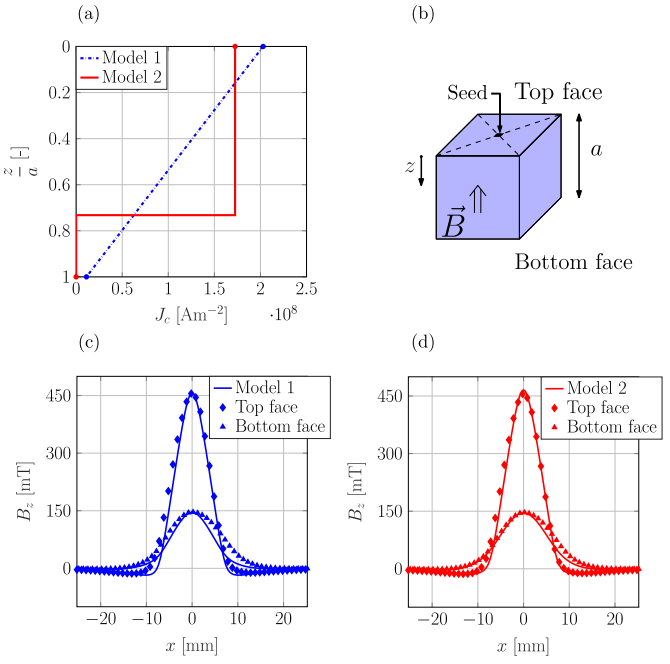

Figure 12. Comparison between the measured trapped field and the analytical model assuming the sample is in the critical state and a field-independent critical current density. Measurements are performed 1 mm away from the surface of sample 2 both above the top and bottom surface. (a) Evolution of J_c along the *c*-axis considered in each analytical model, (b) Geometry and coordinate definition, (c) and (d) Comparison of the experimental data to analytical Model 1 and 2 respectively.

It can be observed in Figure 12 that both over-simplified $J_c(z)$ dependence give results that are in excellent agreement with the measured trapped field distribution for a small computational effort. It should nevertheless be noted that trapped field measurements are mainly sensitive to the current loops close to the surface above which the Hall probe the mapping is performed. It is therefore impossible to determine which J_c distribution is the most appropriate using Hall probe mapping measurements only, since both $J_c(z)$ lead to very similar distributions.

In order to access an experimental parameter that is able to discriminate the particular J_c distributions shown in Figure 12(a), we consider the magnetic moment, which is proportional to the average value of J_c over the whole bulk superconductor. Using a flux extraction magnetometer design to accommodate large size magnetized samples [54], it is possible to measure experimentally the volume magnetic moment of each sample. The same magnetizing process as for the trapped field measurements is followed and the volume magnetic moment is measured 45 minutes after the end of the magnetization process. The experimental results are presented in Table 3 together with the value computed analytically based on the two J_c distributions considered above.

Table 3. Comparison between the measured magnetic moment of the cuboid bulk superconductors with the values computed analytically. Model 1 assumes a linear variation of J_c along the *c*-axis. Model 2 assumes a constant critical current density followed by an abrupt drop to 0 at a given position along the *c*-axis.

Sample number	Magnetic moment [A m^2] Model 1	Model 2	Magnetometer measurements
1	0.71	0.84	0.97
2	0.85	1.02	1.19
3	0.72	0.81	0.87

It appears clearly in Table 3 that both models lead to an underestimation of the actual magnetic moment of the sample. This observation suggests that the J_c distributions represented in Figure 12 are an oversimplified view of the reality and that a more elaborated distribution could be used. However, given the excellent agreement in terms of trapped flux distribution observed in Figure 12, it is decided to keep the model as simple as possible and to use the model leading to the highest magnetic moment, i.e. Model 2.

Appendix 2: Impact of the non-homogeneity of the critical current density on the field generated by a superconducting Halbach array

The results represented by the black plain line in Figure 11 are compared to a model assuming a constant value of the critical current density over the whole superconductor in Figure 13. In this model, the current density in the central sample is still assumed to be altered over two zones of equal thickness $e = 0.8$ mm. However, the value of the critical current density of each sample is determined by considering the trapped field over the top surface of the superconductor only.

This leads to a significant overestimation both of the trapped field over the bottom surface and of the magnetic moment of each trapped field magnet.

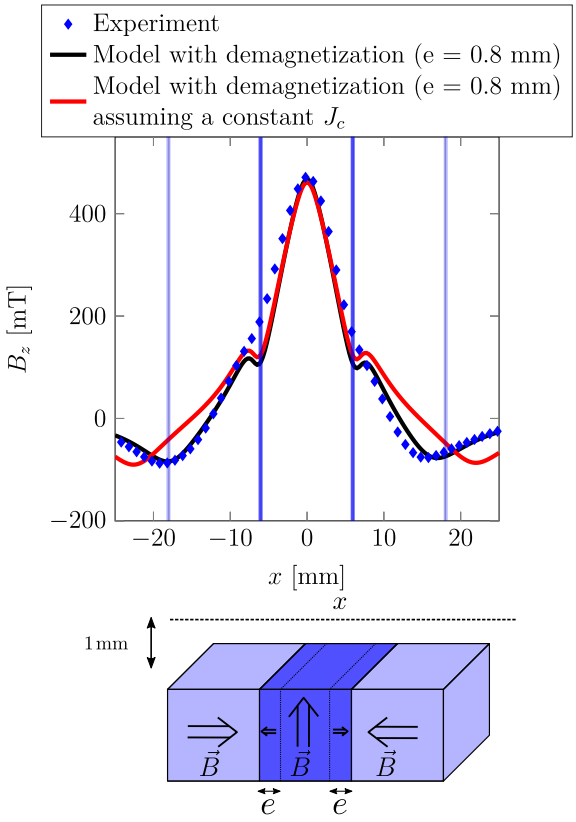

Figure 13. Evolution of the z-component of the magnetic flux density generated 1 mm away from the surface of a Halbach array made up of three cuboid bulk superconductors along the line x. The blue vertical lines are located at the border of the superconducting samples. The model assumes that during the assembly of the configuration the current distribution in the central sample is altered over two zones of equal thickness e as represented schematically in Figure 10. The red curve corresponds to a model assuming a constant critical current density over the whole sample. The black curve corresponds to a model assuming a constant critical current density followed by an abrupt drop to 0 at a given position along the c-axis.

As highlighted in Figure 13, the critical current density uniformity affects significantly the magnetic flux density distribution over the peripheral sample. However, it can be noticed that it has only a small impact on the magnetic flux density profile over the centre of the configuration.

Appendix 3: Magnetic flux density generated by a cubic permanent magnet

The x and z-components of the magnetic flux density generated by a cubic permanent magnet at a point $\vec{P}$ can be expressed as follows:

$$B_x = -\frac{\mu_0\, K_c}{4\pi}\left[\left[\frac{P_y-y}{|P_y-y|}\,\operatorname{arctanh}\left(\sqrt{1+\frac{\alpha^2(\frac{a}{2},z)}{(P_y-y)^2}}\right)\right]_{-\frac{a}{2}}^{\frac{a}{2}}\right]_{-\frac{a}{2}}^{\frac{a}{2}} = f(P_x,P_y,P_z), \tag{10}$$

$$B_z = -\frac{\mu_0\, K_c\left(P_x-\frac{a}{2}\right)}{4\pi|P_x-\frac{a}{2}|}\left[\left[\frac{P_y-y}{|P_y-y|}\arctan\left(\frac{P_z-z}{|P_x-x|\sqrt{1+\frac{\alpha^2(\frac{a}{2},z)}{(P_y-y)^2}}}\right)\right]_{-\frac{a}{2}}^{\frac{a}{2}}\right]_{-\frac{a}{2}}^{\frac{a}{2}} = g(P_x,P_y,P_z). \tag{11}$$

Appendix 4: Magnetic flux density generated by a magnetized cubic superconductor

The x and z-components of the magnetic flux density generated by a cubic magnetized superconductor in the critical state at a point $\vec{P}$ can be expressed as follows:

$$B_x = -\frac{\mu_0\, J_c}{4\pi}\int_0^{\frac{a}{2}}\left[\left[\frac{P_y-y}{|P_y-y|}\,\operatorname{arctanh}\left(\sqrt{1+\frac{\alpha^2(x,z)}{(P_y-y)^2}}\right)\right]_{-\frac{L(x)}{2}}^{\frac{L(x)}{2}}\right]_{-\frac{a}{2}}^{\frac{a}{2}}\mathrm{d}x = f^*(P_x,P_y,P_z), \tag{12}$$

$$B_z = -\frac{\mu_0\, J_c}{4\pi}\int_0^{\frac{a}{2}}\frac{P_x-x}{|P_x-x|}\left[\left[\frac{P_y-y}{|P_y-y|}\arctan\left(\frac{P_z-z}{|P_x-x|\sqrt{1+\frac{\alpha^2(x,z)}{(P_y-y)^2}}}\right)\right]_{-\frac{L(x)}{2}}^{\frac{L(x)}{2}}\right]_{-\frac{a}{2}}^{\frac{a}{2}}\mathrm{d}x = g^*(P_x,P_y,P_z). \tag{13}$$

The magnetic flux density by a cubic magnetized superconductor in the critical state at the particular points $\vec{P}_1$ and $\vec{P}_2$ can be expressed as follows:

$$B_z^{P_1} = \frac{\mu_0\, J_c\, a}{\pi}\left[\arctan\left(\sqrt{\frac{2}{3}}\right) - \ln\left(\frac{\sqrt{6}+1}{\sqrt{6}-1}\right) + \sqrt{2}\ln\left(\frac{1+\sqrt{3}}{\sqrt{2}}\right)\right] = 0.2384\times\mu_0\, J_c\, a, \tag{14}$$

$$B_z^{P_2} = \frac{\mu_0\, J_c\, a}{2\pi}\int_{-1}^{1}\arctan\left(\frac{\sqrt{2}\sqrt{x^2+x+1}}{x\,(x+1)}\right)\mathrm{d}x \simeq 0.0375\times\mu_0\, J_c\, a. \tag{15}$$